FEBS Letters 479 (2000) 118–122 FEBS 23961

Three-dimensional NMR structure of the sixth ligand-binding module of the human LDL receptor: comparison of two adjacent modules with different ligand binding specificities[1]

Daniel Clayton[a], Ian M. Brereton[b], Paulus A. Kroon[a], Ross Smith[a,*]

[a] *Department of Biochemistry, University of Queensland, Brisbane, Qld. 4072, Australia*
[b] *Centre for Magnetic Resonance, University of Queensland, Brisbane, Qld. 4072, Australia*

Received 1 June 2000; revised 26 June 2000; accepted 26 June 2000

Edited by Thomas L. James

Abstract The sixth ligand-binding module of the low-density lipoprotein receptor contributes to the binding of apolipoprotein B100-containing lipoproteins. ^{1}H NMR spectroscopy, DYANA and X-PLOR structure calculations were used to determine that this module has a well defined structure with a backbone conformation similar to other modules. Structures from calculations that simulated the presence of a calcium ion showed increased resolution without large increases in energy, increased deviations from idealised geometry or violations of experimental constraints. Investigation of the surface properties of this module indicates there are significant differences from the fifth module, which binds apolipoprotein E-containing lipoproteins in addition to apolipoprotein B100-containing lipoproteins.

Key words: Low-density lipoprotein receptor; Ligand-binding domain; Ligand specificity; Surface property; Nuclear magnetic resonance spectroscopy; Three-dimensional structure

1. Introduction

The low-density lipoprotein receptor (LDLR) is a endocytotic cell-surface receptor that has a central role in the internalisation of apolipoprotein E (apoE)- and apolipoprotein B100 (apoB100)-containing lipoproteins [1,2]. One of the common features of receptors in the LDLR family is a number of cysteine-rich ligand-binding (LB) modules at the N-terminus. Moderate sequence identity (40–50%) is observed across the seven LB modules of the LDLR and six cysteines, one isoleucine, one phenylalanine and two acidic residues included in an S-D-E motif are invariant. Several hydrophobic, and additional acidic residues are also highly conserved across these modules. The crystal structure of LB5 indicates that many of the conserved acidic residues are involved in the coordination of a calcium ion [3], which has been shown to be essential for both correct folding and maintenance of the three-dimensional structure of LB modules [4,5].

The three-dimensional structures of LB1, LB2 [6,7] and LB5 [3] of the LDLR, and CR3 and CR8 [8,9] of the LDLR receptor-related protein have been determined. All of these structures share a I–III, II–V, IV–VI disulphide arrangement and a backbone fold consisting of two loops, the first containing two short segments in β-conformation and the second containing the calcium ion binding site. A short 3^{10} helix is observed after the first loop in all modules while a second short 3^{10} helix is observed after the second loop only in LB5. The first disulphide bond connects the N-terminus of the module to the first loop, the second connects the two loops, and the third connects the calcium-binding loop to the C-terminus. The conserved I and F residues contribute to a small hydrophobic core in LB modules. Obvious differences between modules are a longer first loop in LB2 due to an additional two residues and an increased flexibility in this loop [7]. Differences in the backbone conformation of the calcium-binding loop are also observed between the modules.

Although the LDLR modules are structurally similar, their ligand-specificity is varied. Studies on mutant receptors showed that LB3–7 are required for high affinity binding of apoB100-containing lipoproteins [10–12]. More recent studies on naturally occurring mutant LDL receptors from familial hypercholesterolaemia patients indicate that LB1 and LB2 are also required for the binding of apoB100-containing lipoproteins [13,14]. The binding of apoE-containing lipoproteins to the LDLR, however, is mediated primarily by LB5 [12]. LB6, an adjacent and structurally independent [15] module, does not bind apoE-containing lipoproteins [12]. In this communication we describe the three-dimensional NMR structure of LB6 and compare its surface features with those of LB5. This comparison indicates differences in surface charge and hydrophobicity that may account for their ligand-specificity.

2. Materials and methods

2.1. Peptide synthesis, folding and purification

LB6 was prepared by solid-phase peptide synthesis using *t*-Boc-protected amino acids and standard side chain protecting groups. The dinitrophenyl (DNP) protecting group on the histidine residue was removed with a solution of 20% (v/v) 2-mercaptoethanol, 10% (v/v) diethylamine (DIEA) in dimethylformamide (DMF). Other pro-

*Corresponding author. Fax: (61)-7-3365 4699.
E-mail: ross@biosci.uq.edu.au

[1] Coordinates of the NMR ensemble have been deposited in the Research Collaboratory for Structural Bioinformatics (RCSB) Protein Data Bank, under the accession code 1F82.

Abbreviations: LDLR, low-density lipoprotein receptor; LB, cysteine-rich modules of the ligand-binding domain of LDLR; TOCSY, total correlation spectroscopy; NOESY, nuclear Overhauser effect spectroscopy; DQF-COSY, double-quantum filtered correlation spectroscopy; E-COSY, exclusive correlation spectroscopy; DYANA, dynamics algorithm for NMR applications; VDW, van der Waals; rmsd, root mean square deviation

0014-5793/00/$20.00
PII: S0014-5793(00)01842-1

tecting groups were removed upon peptide cleavage from the resin with anhydrous hydrofluoric acid at 273 K in the presence of the scavengers *p*-cresol and *p*-thiocresol. LB6 was folded in the presence of 3 mM reduced and 0.3 mM oxidised glutathione in 50 mM Tris–HCl buffer, pH 8.5, containing 150 mM NaCl and 25 mM $CaCl_2$ in the absence of oxygen for 3 days at 4° C [5]. Purification was by reverse-phase HPLC on a 22 mm×250 mm C18 column using a 15–30% acetonitrile gradient in 0.1% trifluoroacetic acid over 160 min. LB6 was identified by electrospray mass spectrometry.

2.2. NMR spectroscopy

NMR experiments on LB6 were performed on a Bruker DMX 750 spectrometer (Bruker, Karlsruhe, Germany) at either pH 5.50 and 298 K or pH 6.70 and 288 K, in the presence of 10 mM $CaCl_2$, 1 mM 3,3,3-trimethylsilylpropionate (TSP) and 10% deuterium oxide (D_2O) (99.9% isotopic purity, Wilmad, Buena, NJ, USA). Total correlation spectroscopy (TOCSY) [16], nuclear Overhauser effect spectroscopy (NOESY) [17] and phase-sensitive COSY [18] spectra were recorded using TPPI for quadrature detection in the F1 dimension. Water suppression was achieved in the TOCSY and NOESY experiments by using the WATERGATE 3-9-19 pulse sequence [19] and by low power presaturation during the recycling delay in the COSY experiment. Exclusive correlation spectroscopy (E-COSY) experiments for determining the χ^1 angle constraints were performed in 99.9% D_2O. Spectra were transformed using XWINNMR software (Bruker) with either $\pi/2$ or $\pi/3$ shifted sine-bell apodisations then baseline corrected. To identify backbone amide protons having reduced exchange rates a series of short two-dimensional TOCSY spectra were acquired after lyophilising and redissolving a sample of LB6 at pH 5.50 in 99.9% D_2O. Amide protons having significant signal remaining after 1.5 h were classed as having a reduced exchange rate.

2.3. NMR distance and angle constraints

Proton resonances were referenced to TSP and assigned manually from TOCSY, COSY and NOESY spectra, and by using the XEASY software package [20]. Elliptical volume integration was performed on a 100 ms mixing time NOESY spectrum, recorded at pH 5.50, using XEASY software. The CALIBA macro of dynamics algorithm for NMR applications (DYANA)-1.5 [21] was used to convert volumes to upper distance limits then pseudoatom corrections were introduced where stereospecific assignments were not available [22]. NOEs observed on a 200 ms spectrum but not on the 100 ms spectrum were included in structure calculations as distance constraints with an upper limit of 6.0 Å. NH-αH coupling constants were determined from the double-quantum filtered correlation spectroscopy (DQF-COSY) spectrum using a Lorentzian line-fitting routine in the Aurelia (Bruker) software. Coupling constants greater than 8 Hz were used in structure calculations as ϕ angle constraints of $120 \pm 30°$. χ^1 angle conformations were determined from the pattern of αH-βH/β′H coupling constants and intraresidue αH-βH/β′H and NH-βH/β′H NOE intensities [23], and introduced as constraints of $-60 \pm 30°$ (*gauche* +), $60 \pm 30°$ (*gauche* −) and $180 \pm 30°$ (*trans*).

2.4. Structure calculations

192 intraresidue, 261 medium-range (≤4 residues) and 104 long-range (>4 residues) distance constraints, 18 ϕ and 14 χ^1 angle constraints were used in DYANA-1.5 and X-PLOR [24] structure calculations. Three disulphide bonds (C3–C15, C10–C28, C22–C37) were introduced based on the arrangement determined for LB1, LB2 [25,26] and LB5 [3]. 100 structures were calculated with DYANA-1.5 using 10 000 steps of torsion angle dynamics for each calculation. The 50 structures with the lowest target function (<11) were imported into X-PLOR for simulated annealing, structure refinement and energy minimisation. X-PLOR calculations consisted of 12 000 steps of high temperature dynamics at 1000 K, cooled to 0 K over 6000 steps then 2000 rounds of Powell energy minimisation using a geometric force field (jhparallhdg.pro). The effective energy term for the NOE constraints was 50 kcal mol^{-1} and for dihedral angle constraints was 5 kcal mol^{-1} rad^{-2} during high temperature dynamics and 200 kcal mol^{-1} rad^{-2} during the cooling and minimisation stages. A further 3000 steps of Powell energy minimisation were performed in a full force field (jhh3x.pro).

2.5. Inclusion of the calcium ion

The X-PLOR topology and structure parameters for Ca^{2+} were obtained from the Hetero-compound Information Centre-Uppsala (http://alpha2.bmc.uu.se/hicup). The sidechains involved in calcium coordination and the calcium to oxygen distances were based on those in the crystal structure of LB5 [3]. Sidechain carboxyl groups (D23, D27, D33, E34) were included in structure calculations as upper distance limits of 2.5 Å and carbonyl groups (R20, E25) were included as upper limits of 2.3 Å.

2.6. Structural statistics and molecular modelling

X-PLOR software was used to determine the bond, angle, van der Waals (VDW) and experimental NOE and dihedral energy of the NMR ensemble. Procheck-NMR [27] was used to determine deviations from idealised geometry and experimental constraints, and generate Ramachandran plots to assess the quality of the structures. MOLMOL 2.6 [28] was used to determine root mean square deviation (rmsd) values for overlays, and InsightII software (Molecular Simulations Inc, San Diego, CA, USA) was used to generate the solvent-accessible Connolly surface of LB5 and LB6 and to visualise the distribution of surface charge and hydrophobicity.

Table 1
Structural statistics for the 20 lowest energy LB6 structures calculated in the absence and presence of different combinations of calcium ligands[a,b]

	No ligands	Four equatorial ligands	Five equatorial ligands	Five equatorial ligands Two apex ligands
Energies (kcal mol^{-1})				
overall	−52 ± 3	−44 ± 3	−42 ± 3	−36 ± 2
VDW	−220 ± 5	−213 ± 4	−217 ± 2	−212 ± 4
NOE	44 ± 1	45 ± 1	47 ± 1	49 ± 1
Rmsd from idealised geometry				
bonds (Å)	0.012 ± 0.0002	0.011 ± 0.0002	0.011 ± 0.0001	0.011 ± 0.0001
angles (°)	2.58 ± 0.02	2.56 ± 0.02	2.60 ± 0.02	2.59 ± 0.02
impropers (°)	0.24 ± 0.01	0.23 ± 0.01	0.24 ± 0.01	0.25 ± 0.01
Rmsd from experimental restraints				
noe (Å)	0.051 ± 0.0004	0.052 ± 0.0005	0.053 ± 0.0003	0.054 ± 0.0004
cdih (°)	0.38 ± 0.04	0.38 ± 0.03	0.41 ± 0.04	0.42 ± 0.03
Ramachandran plot regions				
in favoured (%)	71.7	71.7	72.7	72.1
in additionally allowed (%)	26.8	25.0	22.0	24.4
in generously allowed (%)	1.1	3.3	4.8	3.5
in disallowed (%)	0.5	0	0.5	0
Rmsds for overlays (Å) (backbone, all)				
3–37	0.38, 0.95	0.30, 0.81	0.30, 0.83	0.27, 0.83
3–19	0.18, 0.65	0.19, 0.63	0.19, 0.64	0.17, 0.63
20–34	0.28, 1.11	0.18, 0.88	0.19, 0.93	0.17, 0.96

[a]None of the structures have NOE violations greater than 0.3 Å or angle violations greater than 2°.
[b]Energy and rmsd values are stated as average ± standard deviation.

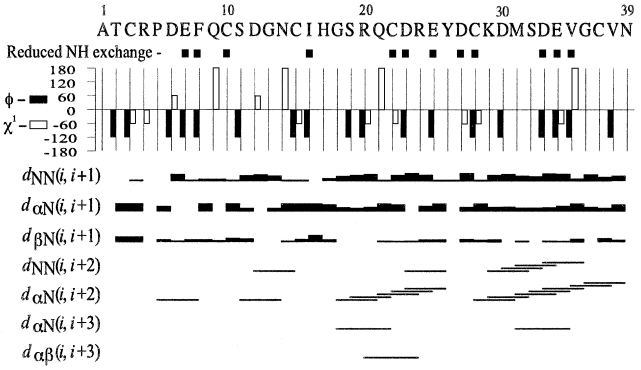

Fig. 1. Summary of distance constraints, angle constraints and amide proton exchange data for LB6. Bar heights shown for the NN(i, i+1), αN(i, i+1), βN(i, i+1) constraints are proportional to the NOE intensities observed. Only the presence, not the magnitude, of NN(i, i+2), αN(i, i+2), αN(i, i+3) and αβ(i, i+3) constraints is indicated.

3. Results and discussion

3.1. Experimental constraints and deuterium exchange experiments

The data derived from NMR experiments on LB6 are summarised in Fig. 1. Amide protons having a reduced exchange rate are E7, F8, C10, I16, C22, D23, E25, D27, C28, D33, E34 and V35. Of these, E7, F8 and I16 had a significant signal remaining after 2.5 days. Both of the fully conserved hydrophobic residues (F8, I16) and 5 (D23, E25, D27, D33, E34) out of six residues that correspond to those involved in calcium coordination in LB5 [3] have amide protons with a reduced exchange rate. All of the corresponding residues of LB1 [6] and of the C-terminus of LB2 (recent unpublished data) have reduced amide proton exchange rates.

3.2. Secondary structure determination

Although sequence conservation, similarity in backbone fold and amide exchange rates between LB1, 2 and LB6 indicate an identical pattern of calcium coordination to LB5, a cautious approach was taken to the introduction of constraints for calcium. Initially structures were calculated in the absence of calcium, then it was introduced with constraints to four conserved equatorial carboxyl ligands (D23, D27, D33 and E34). Distance constraints to both of the carboxyl oxygen atoms on the last equatorial ligand (E34) were then included to investigate the possibility of a pentagonal bipyramidal ligand arrangement. This is more commonly observed than an octahedral arrangement in calcium-binding proteins [29], and may be important in conferring calcium specificity [30]. The two backbone carbonyl groups (R20, E25) which serve as the apex ligands in LB5 were then introduced into structure calculations.

The structure of LB6 (Fig. 2a,c) calculated in the absence of calcium shows a similar overall backbone fold to other modules [3,6,7]. The Kabsch and Sander [31] secondary structure search algorithm in MOLMOL 2.6 did not, however, identify any regions of 3^{10} helix in structures generated in the absence of calcium. The rmsd for overlay of backbone atoms between C3 and C37 on the mean structure is 0.38 Å and for all heavy atoms is 0.95 Å (Table 1). Structures calculated with inclusion of distance constraints for the four equatorial ligands showed only minor differences in backbone conformation from those calculated without such constraints (Fig. 2b). This family of structures was, however, better defined than those calculated without explicit introduction of the calcium ion ligands, having a rmsd of 0.30 Å for overlay of backbone atoms and 0.81 Å for all heavy atoms over the same region (Table 1). The number of NOE constraints per residue is high (Fig. 3a) and backbone ϕ and ψ angles have uniformly high ($\phi > 0.95$, $\psi > 0.94$) angle order parameters (S^{angle}) [32] from the first to the last cysteine residue. Furthermore, 27 of the 31 χ^1 angles in this region have S^{angle} values greater than 0.90 (Fig. 3b). As expected, the biggest increase in backbone resolution is in the calcium-binding loop, between R20 and E34. In this segment, the rmsd value for backbone atom overlay decreased from 0.28 Å to 0.18 Å and from 1.11 Å to 0.88 Å for all heavy atoms. A slight increase in the VDW energy of the structures was observed but this is probably due to the inclusion of the VDW radius of the calcium ion into structure calculations. The inclusion of the calcium ion did alter ϕ and ψ angles enough to result in the Kabsch and Sander secondary structure search routine identifying a region of 3^{10} helical structure after the second loop, between S32 and E34 (Fig. 2c). This helix is also identified in LB5 [3] but not in LB1 or LB2 (recent unpublished data). One region of helical structure, identified in LB1, LB2 and LB5 but not LB6, is the short 3^{10} helix located after the fully conserved hydrophobic residue, I16. Inspection of the ϕ and ψ angles from G18 to R20, however, indicates that this region can be classified as a 3^{10} helix with ϕ angles between $-56°$ and $-90°$ and ψ angles between $-6°$ and $-20°$ [33].

Including both carboxyl groups of E34 as calcium-ion ligands did not result in a significant change in the energy, Ramachandran plot statistics or rmsd values (Table 1). When the two carbonyl apex ligands were introduced into structure calculations a small increase in VDW energy was

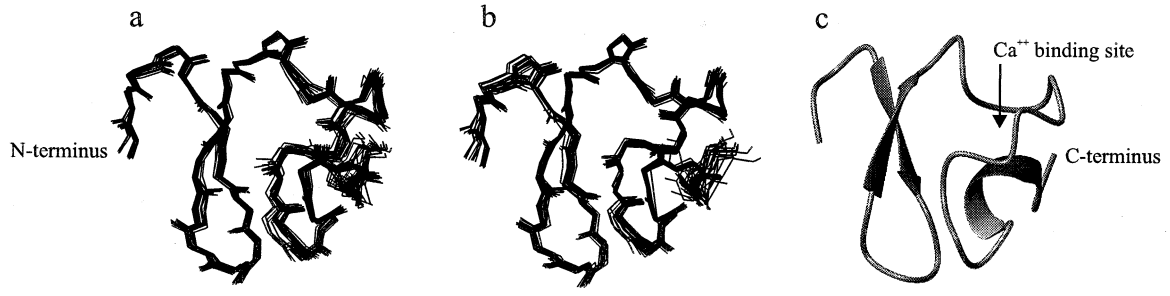

Fig. 2. The 20 lowest energy structures of LB6 calculated in (a) the absence of constraints for the calcium ion and (b) the presence of distance constraints for the four conserved acidic residues corresponding to those identified to be equatorial Ca^{2+} ligands in LB5. c: Shows secondary structural elements identified in structures shown in (b).

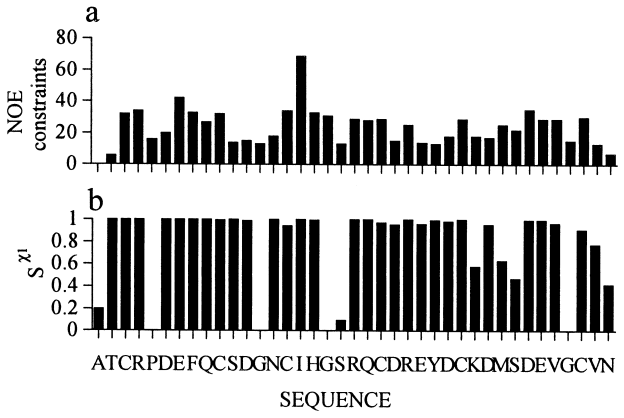

Fig. 3. Plots showing the (a) number of distance constraints per residue and (b) angle order parameter values (S^{angle}) for χ^1 angles.

observed, reducing the total energy from −42 kcal mol^{-1} to −36 kcal mol^{-1}. However, there were still no distance or angle constraint violations in these structures greater than 0.3 Å or 2° and more than 96% of the backbone torsion angles were in the most favoured and additionally allowed regions of the Ramachandran plot (Table 1).

In general, the rmsds, energies, geometry and Ramachandran statistics are good for all the calculated structures of LB6. Including the calcium ion in the structural calculations did not result in any large increase in the energy or incur any distance or angle violations: the experimental constraints are consistent with a similar pattern of calcium ligands to LB5. During the preparation of this manuscript a NMR structure of a mutant of LB6 was published [34], the structure of the wild type LB6 described in the present communication has lower overall energy, lower rmsd values and significantly better Ramachandran plot statistics.

3.3. Comparison of LB5 and LB6

Since all of the LB modules show a similar backbone structure, and most of the conserved residues are involved in either calcium coordination or formation of the small hydrophobic core it is expected that non-conserved residues present on the surface of the modules confer ligand specificity. This point is particularly relevant to LB5, the module which contributes the most to binding of apoE-containing lipoproteins; what features of LB5 result in its dominant role in apoE binding? As mentioned previously, LB6 is an adjacent and structurally independent LB module that is not required to bind apoE-containing lipoproteins. The LB6 structure described here is well defined in terms of both backbone (Table 1) and sidechain resolution (Fig. 3b), allowing us to accurately determine the positioning of surface charge and hydrophobicity and compare it to that of LB5. Residues unique to LB5 that are located on the surface of the module may have a role in conferring ligand specificity.

Residues between the first and last cysteine that are unique to LB5 are A7, F8, H11, L13, S20, G27, K33, E37 and N38 (top of Fig. 4). Of these, the presence of F8, L13, K33 or E37 results in the addition of a charged functional group or of a large non-polar sidechain to LB5. Fig. 4 shows the surface charge and hydrophobicity resulting from basic (blue), acidic (red) and large non-polar (F, I, L, M, V, W (green)) sidechains in LB5 and LB6. The hydrophobic patch obvious on the surface of LB5 viewed in Fig. 4a, but not LB6 (Fig. 4d), is due to a tryptophan residue (W22) not unique to LB5. Also evident on both modules are regions of negative charge arising from conserved acidic residues (D25, D29 (LB5): D23, D27 (LB6)) involved in calcium ion binding (Fig. 4a,d, right of top

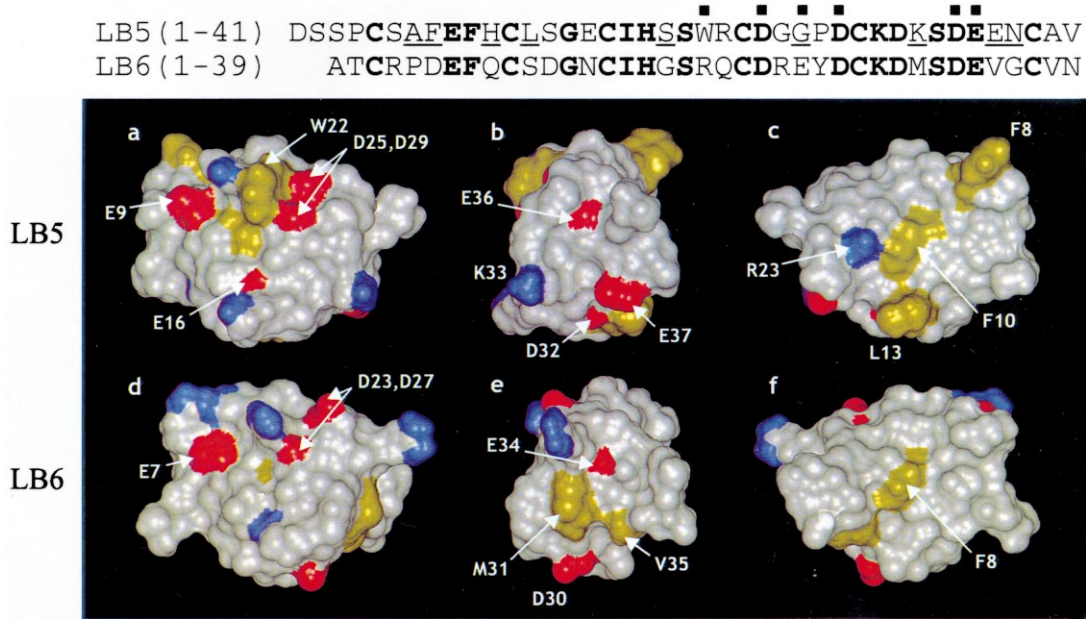

Fig. 4. Primary sequence and distribution of surface charge and hydrophobicity in LB5 and LB6 (lowest energy structure). Residues shown in bold are common to both modules; residues marked with filled squares are coordinated to calcium in LB5; and those underlined are unique (across all modules) to LB5 between the first and last cysteine residue. Modules in a and d have an similar orientation to that of Fig. 2, then are shown (left to right) rotated in two anticlockwise 90° steps, as viewed from the bottom, around the vertical axis. Positively charged functional groups are shown in blue, negatively charged groups are shown in red, and the sidechains of large non-polar residues (F, I, L, M, V, W) are shown in green.

centre), and from acidic residues in the N-terminal, E9 (LB5) and E7 (LB6) (Fig. 4a,d, left of top centre). An additional region of negative charge is present on LB5 due to E16 (Fig. 4a, below centre), making it the only LB module in the LDL receptor to have negative charge at both the E9 and E16 sequence positions, a combination that may contribute to the ability of LB5 to bind basic residues in the receptor-binding region of apoE. Anticlockwise rotation by 90°, as viewed from the bottom, of the modules around the vertical axis shows two residues (K33, E37) on LB5 whose presence results in a unique region of surface charge (Fig. 4b, below centre, right and left). E37 contributes additional negative charge to the surface of LB5, which may be important to this module's electrostatic attraction to the positively charged apoE. Though this attraction is thought to be primarily between acidic residues in LB5 and basic residues in apoE [35], K33 may interact with acidic residues such as E131, E132 and D151 in the receptor-binding region of apoE. In LB6, K33 is replaced by a hydrophobic methionine (M31) while E37 is replaced by a valine residue (V35) (Fig. 4e, below centre), resulting in the presence of a hydrophobic patch on LB6. Positioned below this methionine residue is an aspartate residue (D30) which is not involved in calcium coordination but is conserved in six of the seven LDLR modules. This aspartate residue (D32) is present in a similar position in LB5 but appears to be less solvent-exposed (Fig. 4b). Negative charge from a conserved glutamate residue that is involved in calcium binding (E36 (LB5): E34 (LB6)) is also evident on both modules (Fig. 4b,e). Fig. 4c,f shows the modules after a further 90° anticlockwise rotation. The positive charge obvious in Fig. 4c results from the presence of R23, a residue not unique to LB5. A patch of surface hydrophobicity resulting from the edge of the fully conserved phenylalanine residue (F10 (LB5): F8 (LB6)) (Fig. 4c,f, centre) is evident on both modules. The additional presence of F8 and L13, in LB5, results in an almost continuous strip of surface hydrophobicity running from the top right to the centre bottom of the module (Fig. 4c), a feature previously identified [3]. It is of note that these two large non-polar residues which are unique to LB5 have a large proportion of their sidechains exposed to the solvent.

In conclusion, rmsd values listed in Table 1 indicate that this is the best-defined NMR structure of an LB module reported to date. Comparison of the solvent-exposed surface of LB5 and LB6 indicates several unique features of the surface of LB5 that may allow it to bind apoE in addition to apoB100; positive charge resulting from K33; negative charge resulting from E37; the presence of negative charge at both E9 and E16, and a strip of surface hydrophobicity resulting from F8, F10 and L13. A region of high negative electrostatic potential is present on the surface of both modules. In LB5, a combination of this and one or more of the features listed above may result in its ability to bind apoE-containing lipoproteins. Further experiments, such as studies on the effects of site-directed mutagenesis of LB5 on the interaction with apoE, could clarify the contribution of these residues to lipoprotein–receptor binding.

Acknowledgements: This work was supported by a grant to P.A.K., R.S. and I.M.B. from the Australian National Health and Medical Research Council. Thanks also to Drs S.B.H. Kent and J. Wilkins of Gryphon Sciences, San Francisco, for use of their facilities and guidance with the peptide synthesis.

References

[1] Mahley, R.W. and Innerarity, T.L. (1977) J. Biol. Chem. 252, 3980–3986.
[2] Brown, M.S. and Goldstein, J.L. (1986) Science 232, 34–47.
[3] Fass, D., Blacklow, S., Kim, P.S. and Berger, J.M. (1997) Nature 388, 691–693.
[4] Atkins, A.R., Brereton, I.M., Kroon, P.A., Lee, H.T. and Smith, R. (1998) Biochemistry 37, 1662–1670.
[5] Bieri, S., Atkins, A.R., Lee, H.T., Winzor, D.J., Smith, R. and Kroon, P.A. (1998) Biochemistry 37, 10994–11002.
[6] Daly, N.L., Scanlon, M.J., Djordjevic, J.T., Kroon, P.A. and Smith, R. (1995) Proc. Natl. Acad. Sci. USA 92, 6334–6338.
[7] Daly, N.L., Djordjevic, J.T., Kroon, P.A. and Smith, R. (1995) Biochemistry 34, 14474–14481.
[8] Dolmer, K., Huang, W. and Gettins, P.G. (2000) J. Biol. Chem. 275, 3264–3269.
[9] Huang, W., Dolmer, K. and Gettins, P.G. (1999) J. Biol. Chem. 274, 14130–14136.
[10] Esser, V., Limbird, L.E., Brown, M.S., Goldstein, J.L. and Russell, D.W. (1988) J. Biol. Chem. 263, 13282–13290.
[11] van Driel, I.R., Goldstein, J.L., Sudhof, T.C. and Brown, M.S. (1987) J. Biol. Chem. 262, 17443–17449.
[12] Russell, D.W., Brown, M.S. and Goldstein, J.L. (1989) J. Biol. Chem. 264, 21682–21688.
[13] Sass, C., Giroux, L.M., Lussier-Cacan, S., Davignon, J. and Minnich, A. (1995) J. Biol. Chem. 270, 25166–25171.
[14] Rødningen, O.K., Tonstad, S., Medh, J.D., Chappell, D.A., Ose, L. and Leren, T.P. (1999) J. Lipid Res. 40, 213–220.
[15] North, C.L. and Blacklow, S.C. (1999) Biochemistry 38, 3926–3935.
[16] Bax, A. and Davis, D.G. (1985) J. Magn. Reson. 65, 355–360.
[17] Jeener, J., Meier, B.H., Bachmann, P. and Ernst, R.R. (1979) J. Chem. Phys. 71, 4546–4553.
[18] Marion, D. and Wüthrich, K. (1983) Biochem. Biophys. Res. Commun. 113, 967–974.
[19] Sklenar, V., Piotto, M., Leppik, R. and Saudek, V. (1993) J. Magn. Reson. Ser. A 102, 241–245.
[20] Bartels, C., Xia, T.-H., Billeter, M., Gunter, P. and Wüthrich, K. (1995) J. Biomol. NMR 5, 1–10.
[21] Güntert, P., Mumenthaler, C. and Wüthrich, K. (1997) J. Mol. Biol. 273, 283–298.
[22] Wüthrich, K., Billeter, M. and Braun, W. (1983) J. Mol. Biol. 169, 949–961.
[23] Wagner, G., Braun, W., Havel, T.F., Schaumann, T., Go, N. and Wüthrich, K. (1987) J. Mol. Biol. 196, 611–639.
[24] Brünger, A.T. (1993) X-PLOR Version 3.1: A System for X-Ray Crystallography and NMR, Yale University Press, New Haven, CT.
[25] Bieri, S., Djordjevic, J.T., Daly, N.L., Smith, R. and Kroon, P.A. (1995) Biochemistry 34, 13059–13065.
[26] Bieri, S., Djordjevic, J.T., Jamshidi, N., Smith, R. and Kroon, P.A. (1995) FEBS Lett. 371, 341–344.
[27] Laskowski, R.A., Rullmannn, J.A., MacArthur, M.W., Kaptein, R. and Thornton, J.M. (1996) J. Biomol. NMR 8, 477–486.
[28] Koradi, R., Billeter, M. and Wüthrich, K. (1996) J. Mol. Graph. 14, 29–32.
[29] Strynadka, N.C. and James, M.N. (1989) Annu. Rev. Biochem. 58, 951–998.
[30] da Silva, A.C., Kendrick-Jones, J. and Reinach, F.C. (1995) J. Biol. Chem. 270, 6773–6778.
[31] Kabsch, W. and Sander, C. (1983) Biopolymers 22, 2577–2637.
[32] Hyberts, S.G., Goldberg, M.S., Havel, T.F. and Wagner, G. (1992) Protein Sci. 1, 736–751.
[33] Geetha, V. (1996) Int. J. Biol. Macromol. 19, 81–89.
[34] North, C.L. and Blacklow, S.C. (2000) Biochemistry 39, 2564–2571.
[35] Mahley, R.W. (1988) Science 240, 622–630.